S & M 4163

Development and Field Application of Fracture Detection Technology for Internal Tendons in Prestressed Concrete Bridges Using Acoustic Emission Techniques

Young-Chul Moon, ¹ Soojin Cho, ¹ Dong-Woo Seo, ² Yun-Ki Hong, ³ and Dong-Hyun Kim^{3*}

¹Department of Civil Engineering, University of Seoul,
 163 Seoulsiripdae-ro, Dongdaemun-gu, Seoul 02504, Republic of Korea
 ²Department of Structural Engineering Research, Korea Institute of Civil Engineering and Building Technology,
 283 Goyangdae-ro, Ilsanseo-gu, Goyang-si, Gyenggi-do 10223, Republic of Korea
 ³Research & Development Center, RECTUSON Co., Ltd.
 51756 12-1, Gaposinhangnam-ro, Masanhappo-gu, Changwon-si, Gyeongsangnam-do, Republic of Korea

(Received February 28, 2025; accepted September 4, 2025)

Keywords: acoustic emission, prestressed concrete bridge, grout void, internal tendon, wire break, structural health monitoring

Acoustic emission (AE) techniques are among the most effective nondestructive evaluation (NDE) methods for the structural health monitoring (SHM) of large-scale infrastructure. These techniques enable the real-time monitoring of concrete cracks and damage to embedded steel reinforcements without causing structural failure. In particular, they are well suited for detecting fractures in tendons within prestressed concrete (PSC) bridges. PSC bridges are structurally classified into internal and external tendon systems, depending on their prestressing method. Although external tendons can be inspected through visual or acoustic methods, detecting defects in internal tendons is significantly more challenging owing to their embedded placement within the concrete. This study highlights the application of AE sensor technology as a core sensing method to capture and interpret material-specific fracture signals from both concrete and steel tendons. The distinction between the acoustic characteristics of concrete cracking and tendon breakage requires tailored signal processing techniques that reflect the physical properties of these structural materials. This study aims to develop an AE-based technology for detecting fracture signals in the internal tendons of PSC bridges and to establish maintenance guidelines for safety inspections and field applications. To achieve this, various simulated fracture tests are conducted to build a database of AE signals associated with tendon fractures. Additionally, field experiments are performed on an in-service PSC bridge in Seoul, South Korea, to evaluate the feasibility of real-world implementation. From the results of these field validation tests, maintenance guidelines for the AE-based monitoring of internal tendon fractures in PSC bridges are proposed.

^{*}Corresponding author: e-mail: dhkim@rectuson.com https://doi.org/10.18494/SAM5612

1. Introduction

Acoustic emission (AE) techniques are among the most effective nondestructive evaluation (NDE) methods for the structural health monitoring (SHM) of large-scale infrastructure. These techniques enable the real-time monitoring of concrete cracks and damage to embedded steel reinforcements without causing structural failure. In particular, they are well suited for detecting fractures in tendons within prestressed concrete (PSC) bridges.

PSC bridges are structurally classified into internal and external tendon systems, depending on their prestressing method. Although external tendons can be inspected through visual or acoustic methods, detecting defects in internal tendons is significantly more challenging owing to their embedded placement within the concrete.

Recent studies have explored the detection of AE signal variations caused by external load fluctuations in PSC structures with internal damage. These studies have confirmed the possibility of distinguishing between intact and defective conditions by identifying secondary AE activity.⁽¹⁾

AE signal analysis methods for concrete structures have focused predominantly on the correlation between the average frequency and the roughness average (RA),(2-4) allowing for signal source classification. Further research introduced key evaluation methods such as the ratio of repeated train load to relative maximum load for inspection period (RTRI)⁽⁵⁾ and improved b-value analysis,⁽⁶⁾ both of which have been validated for defect detection. Ohtsu⁽⁷⁾ classified AE signals related to tensile and other types of cracks using the average frequency—RA value correlation method, which was later established as an ISO standard.

Subsequent research has expanded into AE signal measurement and interpretation for steel and concrete structures in PSC bridges. Notable advancements include machine-learning-based PSC structural diagnostics, (8) frequency filter applications for PSC railway structures, (9) and the shear failure analysis of PSC bridges using digital image correlation. (10) It is being applied to various steel and concrete structures, such as in a study on improving the signal analysis performance of PSC structures using the filter technique (11) and a damage analysis of PSC girders using newly developed AE parameters. (12)

Recently, studies have increasingly focused on the potential of using AE techniques for detecting wire breaks in complex and highly attenuated structures such as internal tendons. Shiotani *et al.*⁽¹³⁾ analyzed AE activity during loading in post-tensioned PC structures and were able to identify cable breakage using secondary AE activity, with an average AE signal frequency of less than 50 kHz.

Nair and Cai⁽¹⁴⁾ collected AE data from concrete, steel, and fiber-reinforced polymer (FRP) bridges, and performed qualitative and quantitative intensity analyses to assess bridge damage severity. Their study demonstrated the significance of cumulative AE data analysis in bridge integrity monitoring. Tonelli *et al.*⁽¹⁵⁾ compared AE signal variations with data from linear variable differential transformers (LVDTs) for crack detection and rotary variable differential transformers (RVDTs) for bridge deflection, confirming the detection capability of AE techniques.

Lange et al. (16) conducted a novel study using accelerometers within a 17 kHz range to monitor concrete failure and tendon wire breaks. Unlike conventional AE systems that rely on

sensors operating above 60 kHz, their research employed support vector machine (SVM) training and evaluation, enabling wire break detection over distances exceeding 20 m, thereby extending detection capabilities to external tendons.

Käding et al.⁽¹⁷⁾ conducted experiments on six PSC girders in three stress corrosion cracking (SCC)-prone bridges. They established a reference database distinguishing wire break signals from actual traffic noise and rebound hammer impacts. Their study confirmed that wire break locations exhibit low-frequency energy characteristics below 50 kHz and examined how amplitude, energy, and root mean square (RMS) values could enhance damage detection in noisy environments. One study was conducted on the basis of the assumption that rebound hammer and wire break signals exhibit the same characteristics in PSC to determine how to detect wire fractures and establish a suitable sensor layout. Another study examined how the attenuation behaviors of signals in the longitudinal and transverse directions are affected by structural characteristics such as voids and sensor orientation, providing guidance on the optimal number of sensors and signal verification.⁽¹⁸⁾

Farhadi *et al.*⁽¹⁹⁾ artificially induced tendon damage in two Italian PSC bridges and collected AE signals amidst environmental noise. Their study utilized neural network training to classify defects.

Although these studies were able to demonstrate through experiments the potential for detecting internal tendon fractures, they faced limitations in validating detection capabilities under actual bridge conditions.

Our research study was conducted in response to the 2016 fracture incident involving external tendons in a PSC overpass in Seoul, South Korea, which raised significant concerns regarding PSC bridge tendon safety and management. The primary objective of this study is to develop a defect detection technology for internal tendons embedded within concrete, which are challenging to assess using conventional NDE techniques.

Internal tendons are encapsulated in steel ducts filled with grout and embedded within concrete, making fracture detection highly challenging and limiting the reliability of existing NDE methods. To address this issue, this study designed various experimental specimens simulating real-world conditions to conduct tendon fracture tests and assess defect detection feasibility. Finally, the developed AE-based monitoring system was applied to an actual bridge to validate its effectiveness, and a maintenance guideline for internal tendon safety monitoring and failure detection was proposed.

This study focuses on the integration of AE sensor technology and signal analysis techniques that consider the distinct material properties of concrete and steel tendons. By utilizing high-sensitivity AE sensors, the system is able to distinguish wire break signals from concrete crack signals, which is essential for accurate diagnosis in composite PSC structures. Material-specific signal patterns necessitate advanced filtering and interpretation methods to ensure reliable monitoring in complex, noisy environments.

The AE-based SHM system developed in this study enables the differentiation of wire break signals from concrete cracks in PSC bridges, indicating its applicability to pre-existing damaged structures. Additionally, the capability of the system to detect wire break signals in noisy environments, such as those caused by vehicular traffic, was verified. Key AE features—

including amplitude, rise time, duration, frequency, and cumulative AE energy—were identified and incorporated into maintenance guidelines for PSC bridge internal tendon monitoring.

To develop the AE-based PSC bridge internal tendon fracture monitoring system, a tendon fracture signal database was established through three phases of structural experiments. In Phase I, strand tensile failure and three-point bending tests were conducted on PSC specimens to distinguish concrete crack signals from strand fracture signals, focusing on extracting characteristic frequencies under increasing loads. Phase II involved load application experiments on a decommissioned bridge to simulate internal tendon fractures and load application tests on specimens with artificially induced voids in PSC internal tendons. Additional experiments introduced artificial voids in PSC specimens to examine the secondary AE signals generated by friction between fractured strands and grout within void regions. Finally, in Phase III, an AE-based internal tendon fracture monitoring system was deployed on an in-service PSC box girder bridge to validate the field applicability of the proposed system and incorporate findings into safety management guidelines for PSC bridge maintenance.

2. Experiments and Results

2.1 Phase I experiment

2.1.1 Tensile testing of PSC strands

The objective of this experiment was to analyze the frequency characteristics of the signals generated during strand fracture via a tensile test and to select a suitable AE sensor accordingly. The types and characteristics of the specimens used in the experiment are listed in Table 1.

Each specimen was approximately 80 cm in length (Fig. 1). As shown in Fig. 2, the specimen to be subjected to the tensile test was installed in the upper and lower gripping sections of a 1000 kN tensile testing machine. The AE sensor was attached to the gripping section. The specimen

Table 1 Specifications of PSC structure.

| -r | | |
|-------------------|---------------------------|--|
| Classification | Details | |
| Corrosion level 5 | Mass loss rate = 7.18% | |
| Corrosion level 2 | Mass loss rate = 1.34% | |
| Mechanical damage | 1/3 Damage, Case 1 | |

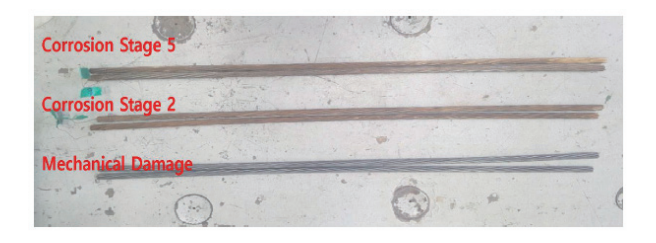


Fig. 1. (Color online) Corrosion and mechanical damage specimens.



Fig. 2. (Color online) Tensile testing machine and sensor installation location.

was subjected to tensile force until fracture occurred, and the characteristics of the AE signals during the experiment were observed.

The experimental results shown in Tables 2 to 4 confirmed that a sensor with a 60 kHz resonance characteristic is appropriate. For comparison, in the case of the 150 kHz resonant sensor, significant signals were detected only at the moment of strand fracture. By contrast, the 60 kHz resonant sensor detected signals related to deformations and minor damage throughout the tensile process.

2.1.2 Characteristics of concrete cracking and internal tendon fracture in PSC specimens

The experiment shown in Fig. 3 was conducted using a PSC specimen containing two prestressed strands (Fig. 4). One strand was completely severed, whereas the other had two wires subjected to intentional mechanical damage. A three-point bending test was performed to differentiate between the acoustic signals of concrete cracking and strand fracture.

Cyclic loading and tensile tests were conducted to collect the signal characteristics of concrete cracking and tendon fracture. The cyclic loading test was used to identify the onset of concrete cracking, whereas the tensile test was used to analyze the signal intensity characteristics during the first and second tendon fractures.

Figure 5(a) shows the AE energy trend during the cyclic loading test. When the maximum load (6.5 tons) was applied, two instances of concrete cracking were observed, with AE energy levels exceeding 1000 aJ compared with the noise level.

Figure 5(b) illustrates the AE energy trend during the tensile test. At approximately 8 tons of load, concrete cracking began to accelerate, with AE energy readings exceeding 10000 aJ. When the load reached 13 tons, the internal strand ruptured, generating a sudden AE energy spike of approximately 48000 aJ.

Table 2 (Color online) Corrosion level 5, mass loss rate = 7.18%.

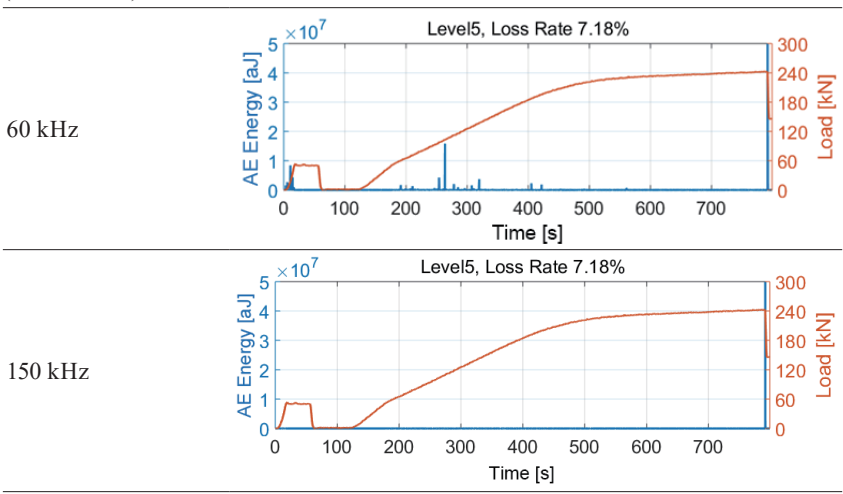


Table 3 (Color online) Corrosion level 2, mass loss rate = 1.34%.

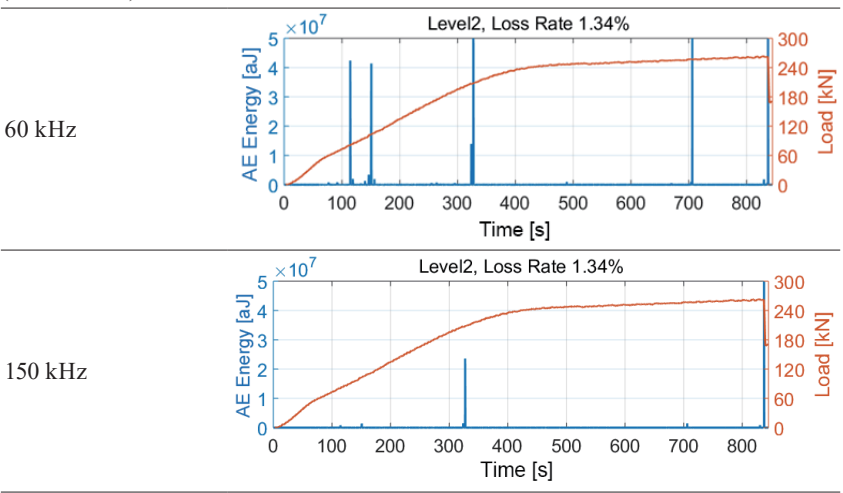


Table 4 (Color online) Mechanical damage, 1/3 damage, Case 1.

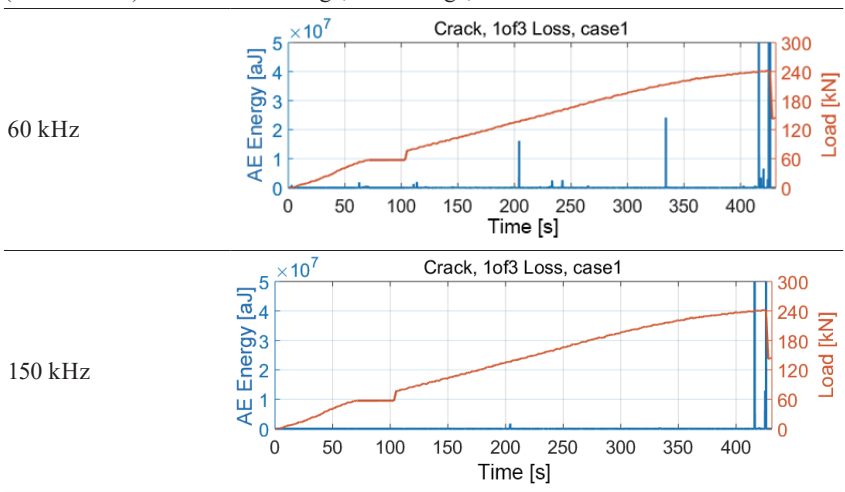




Fig. 3. (Color online) PSC structure defect detection experiment.

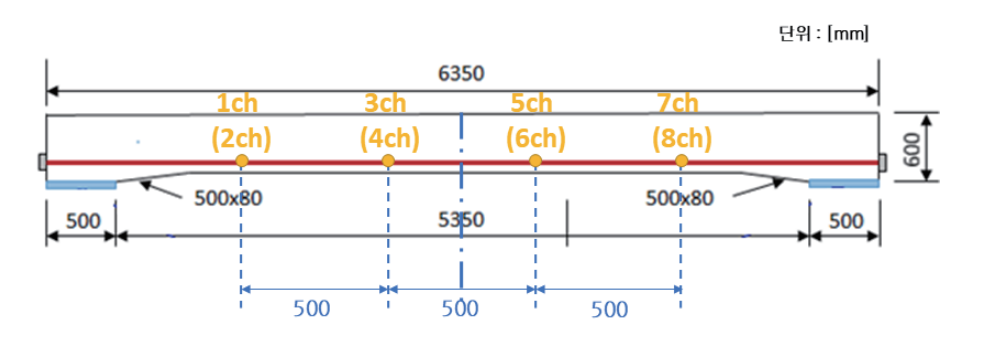


Fig. 4. (Color online) AE sensor installation layout.

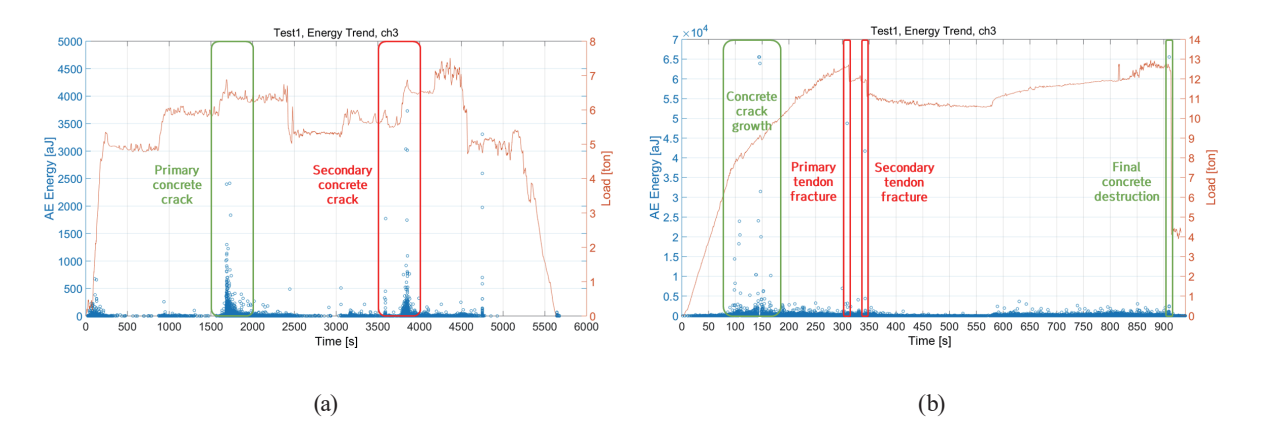


Fig. 5. (Color online) AE energy trends: (a) cyclic load and (b) tensile force experiments.

2.2 Phase II experiment

2.2.1 PSC I-type girder decommissioned bridge experiment

In this experiment, strand fractures were induced in an actual bridge structure to evaluate the detectability of fracture signals. For this purpose, a large-scale specimen was prepared by cutting a portion of a decommissioned I-type girder bridge. As shown in Fig. 6, the strands in the upper-right and lower central sections were partially severed. Load was then applied to induce strand fracture, and the AE signals generated during fracture were recorded.

Figure 7 presents the sensor installation locations marked on a schematic of the PSC structure, along with actual photographs of the installed sensors.

The load application experiment followed the sequence shown in Fig. 8, with cyclic loading applied as illustrated in Fig. 9. A preloading process was conducted to ensure that the concrete was sufficiently stressed while still supported by the tendons. This process induced surface



Fig. 6. (Color online) (a) Upper-right tendon exposure. (b) Lower-central site tendon exposure.

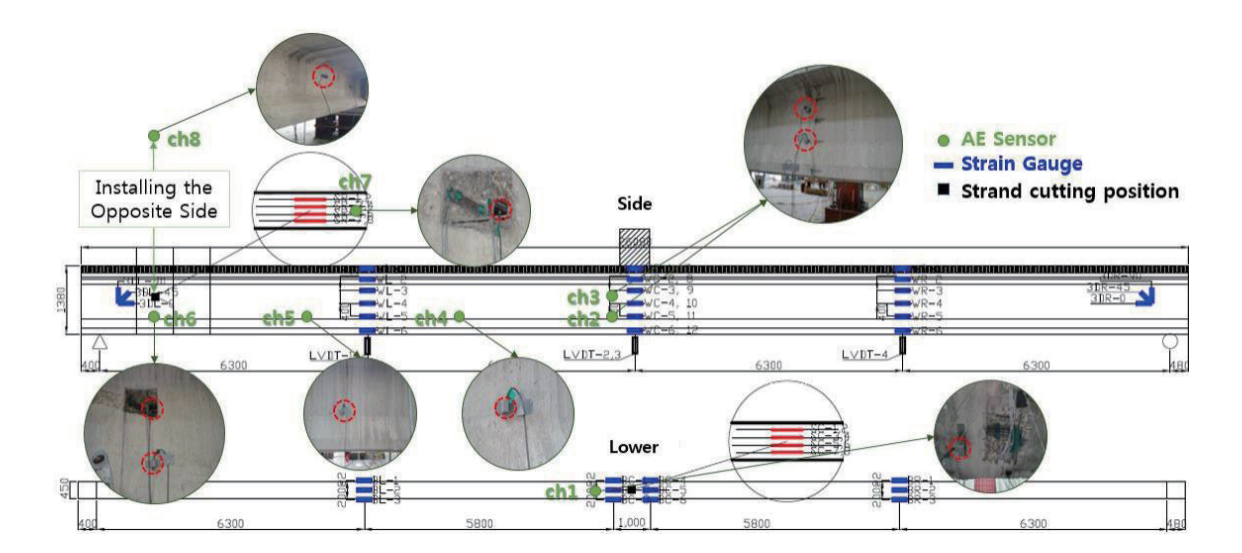


Fig. 7. (Color online) Installation of AE sensor on I-type PSC structure.



Fig. 8. (Color online) Test procedure for internal tendon destructive of I-type PSC structure.

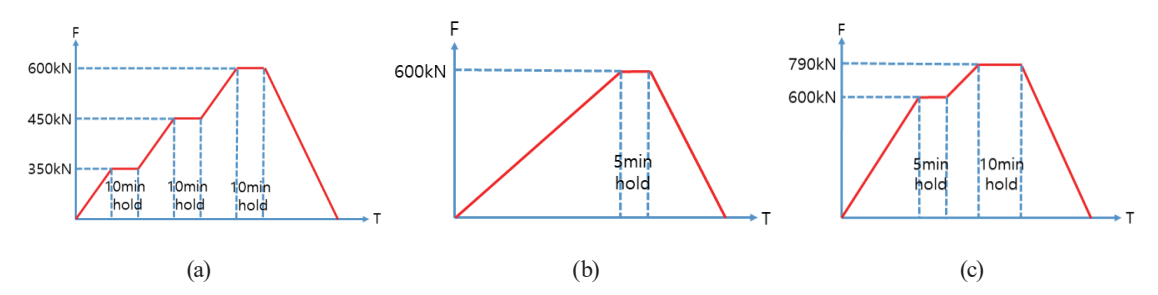


Fig. 9. (Color online) Loading cycle: (a) Preloading. (b) after cutting upper-right strand (1st loading and 2nd loading). (c) after cutting lower-center strand (3rd loading).

cracks in the concrete, weakening the tensile strength of the overall structure. Consequently, when specific strands were cut, the remaining strands, rather than the concrete, bore more of the load, facilitating strand fracture. The detailed preloading cycle is shown in Fig. 9(a).

The strands in the upper-right tendon were severed in two stages. Among the 12 strands, five were exposed at the fracture section. Initially, two of these strands were partially cut prior to the first loading test. Subsequently, the remaining three exposed strands were severed before the second loading test was performed. The loading cycles for the first and second loading tests are shown in Fig. 9(b).

Finally, in the lower central section, three out of the five exposed strands were partially severed before the third loading test was conducted. Similar to the process for the first and second loading tests, the load was initially increased to 600 kN and held for 5 min before being gradually increased to 790 kN. The detailed loading cycle for this test is shown in Fig. 9(c). The loading rate was controlled by displacement at 3 mm per minute.

In the preliminary and first and second loading tests, only the concrete crack patterns could be observed, and no failure due to loading was detected other than the artificially cut strands in the prestressing tendon. A sudden spike in signal was observed at Channel 5, which was unrelated to loading application or tendon failure, suggesting the presence of internal concrete cracks, interface separation, or voids within the tendon.

During the third loading test, a single strand in the lower central section of the tendon ruptured shortly after loading began. The signal from this rupture was transmitted not only to adjacent Channels 1, 2, and 3 but also to Channels 4 and 5. As concrete cracks continued to propagate, an increase in AE activity was observed across Channels 1 to 5.

The second rupture occurred when the load reached 600 kN and was held for 5 min before loading was resumed. As with the first rupture, another strand in the lower central section, where tensile stress was concentrated, fractured. AE energy measurements from Channels 1, 2, 3, and 4 followed a sequential order based on distance. However, the AE energy recorded at Channel 5 (approx. 40000 aJ) exceeded that of Channel 1 (approx. 24000 aJ), which was closest to the rupture point. A similar pattern was observed in subsequent strand failures, where Channel 5 registered a higher AE energy (approx. 33000 aJ) than that observed for Channel 1 (approx. 13000 aJ). This suggests the presence of voids in the tendon near Channel 5. The voids likely provided space for strand movement, allowing greater AE energy to be detected near the void if sudden impact occurred.

As the applied load approached its peak (approx. 790 kN), loud cracking noises were heard from the compressed concrete section at the top of the girder central region.

Figure 10 illustrates the AE energy recorded across all eight channels during the third loading test. The specific events marked in the figure are as follows, with key AE energy values summarized in Table 5.

- (1) First strand rupture
- (2) Load reaches 60 tons and is held for 5 min
- (3) Load increase resumes up to the failure threshold
- (4) Second strand rupture
- (5) Third strand rupture
- (6) Concrete cracking in the upper compression zone (loud noise)
- (7) Ultimate load reaches (79 tons) and is held for 10 min before unloading

The points at which AE activity suddenly increased in Channels 6, 7, and 8—previously showing minimal activity—are shaded in Fig. 10. This is presumed to be secondary AE activity, occurring as the fractured strands in both the upper-right and lower central sections lost support and slipped as a result of tensile loading.

The experiment confirmed that concrete cracking generated AE signals below 10000 aJ, whereas strand ruptures produced AE energy ranging from 10000 to 25000 aJ. Compared with those observed in the initial phase of testing, the strand rupture signals were approximately half as long, likely owing to the effect of corrosion under real-world conditions.

Additionally, extra signals attributed to voids or structural defects were detected, with some even surpassing the AE energy levels of strand ruptures. To further verify these findings, additional experiments were conducted.

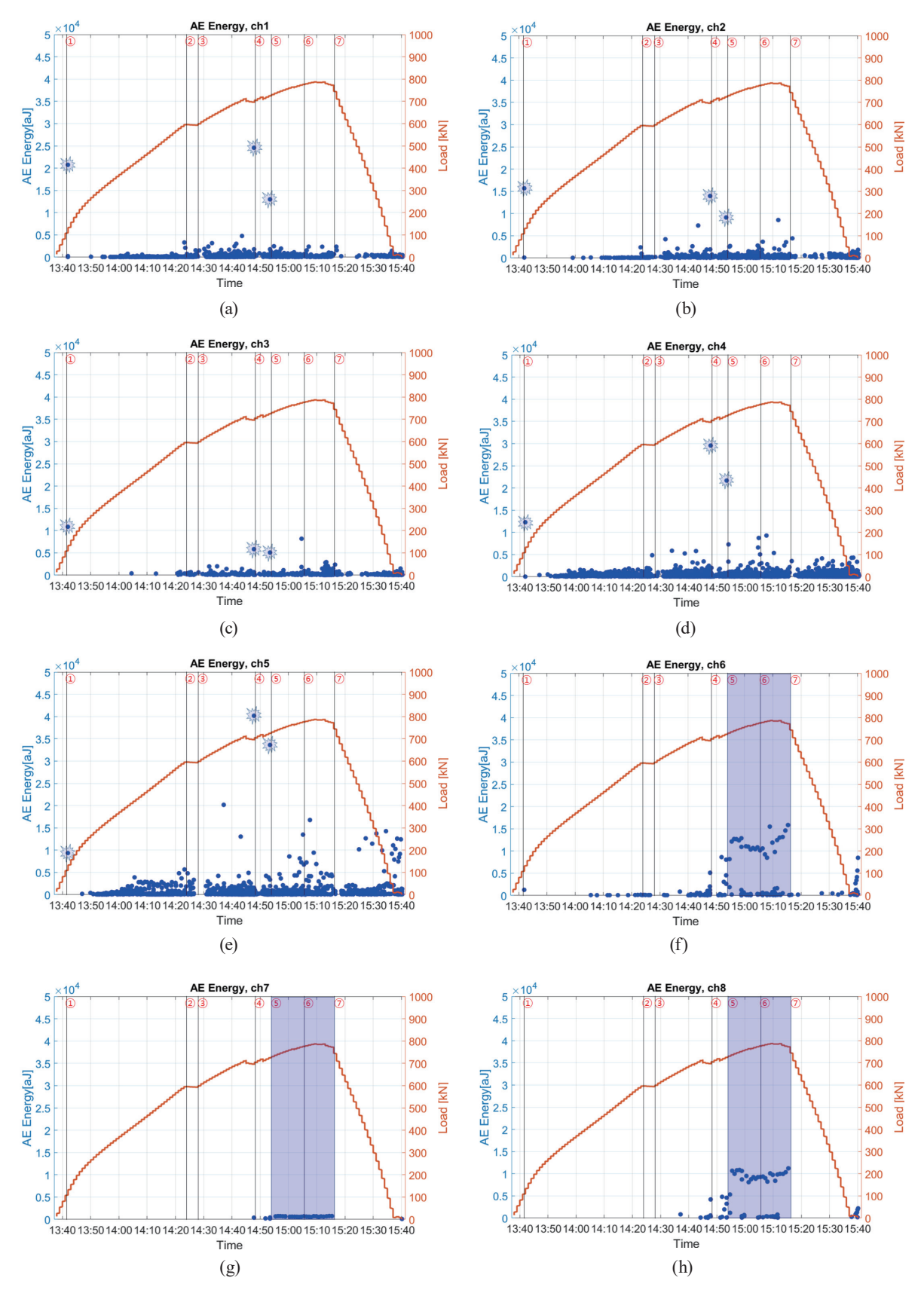


Fig. 10. (Color online) Third loading AE energy trends: (a) ch1, (b) ch2, (c) ch3, (d) ch4, (e) ch5, (f) ch6, (g) ch7, and (h) ch8 trends.

Table 5
AE energy at the time of break of tendon.

| No. | Event | ch1 | ch2 | ch3 | ch4 | ch5 |
|-----|----------------|-------|-------|-------|-------|-------|
| (1) | 1st break | 20743 | 15680 | 10853 | 12285 | 9346 |
| (2) | 2nd break | 24574 | 13947 | 5838 | 29560 | 40181 |
| (3) | 3rd break | 12988 | 9118 | 5079 | 21673 | 33620 |
| (4) | Concrete break | | 2798 | 8182 | 8744 | 13479 |

2.2.2 Simulation of tendon voids in PSC structures

This experiment aimed to replicate the unusual signals observed in the previous I-girder bridge load test and determine their origin. Although an attempt was made to inspect the exact locations where these signals occurred, the test specimens were discarded immediately after the experiment, preventing direct verification. As a result, a similar PSC structural model was created to assess the reproducibility of the signals and investigate their cause.

The primary objective of this experiment was to detect grout voids that may occur during the construction of PSC structures. Specifically, it sought to confirm whether secondary signals generated by strand friction against grout voids within the sheath could be measured using AE techniques. PSC structures are categorized into pretensioned and post-tensioned systems. In post-tensioned systems, steel sheaths are embedded within the concrete before the strands are tensioned, and cementitious grout is injected to protect against strand corrosion. However, owing to various factors, voids may form between the sheath and the strands. These voids allow moisture ingress, potentially leading to strand corrosion, rupture, and structural damage.

For this experiment, PSC test specimens were fabricated using 7-wire prestressing strands inserted into a tendon, as shown in Fig. 11. Figure 12 provides a photograph of the fabricated specimens.

Figure 13 presents the loading cycle, whereas Fig. 14 illustrates the AE energy graph in relation to the actual applied load. The test involved increasing the load at a constant rate while incorporating periods where the load was maintained for a certain duration upon event detection. The maximum load was applied until the displacement between the tensile region at the concrete center and bottom reached a critical level.

Figure 13(a) marks the point where the preloading test exceeded its maximum load. Existing concrete cracks reopened and became visible, and additional crack propagation was observed.

Figure 13(b) represents the phase where concrete cracks continued to grow. Numerous signals were detected primarily in the tensile region at the lower-center part of the concrete.

Figure 13(c) corresponds to the occurrence of strand rupture. This event weakened the tendon supporting the structure, causing cracks to rapidly propagate throughout the structure.

Figure 13(d) refers to a segment where, after strand rupture, the load was not maintained but continuously increased. In this section, distinctive signals were recorded only at ch.1, ch.2, and ch.3, appearing sequentially in the order of ch.3, ch.2, and ch.1, with ch.2 showing the highest AE energy. This suggests that the signal source was closer to ch.3 than to ch.1 but adjacent to ch.2. The estimated signal source location is indicated in Fig. 15. However, no visible signs of

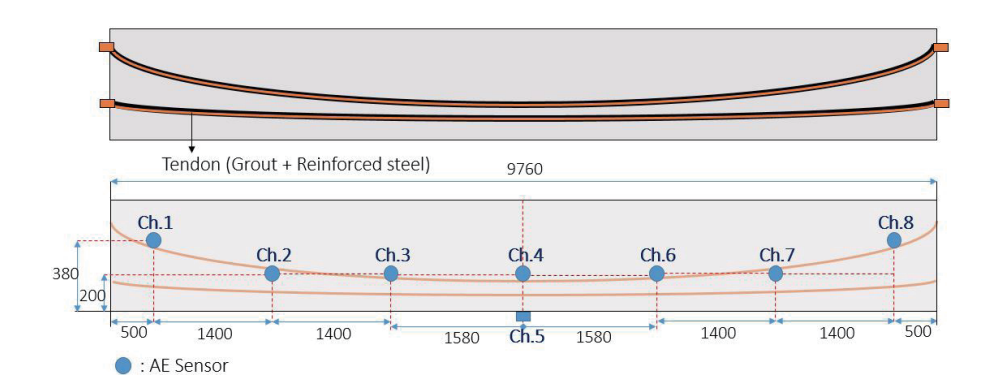


Fig. 11. (Color online) AE sensor layout of PSC specimen in void grouting detection test.



Fig. 12. (Color online) PSC specimen in void grouting detection test.

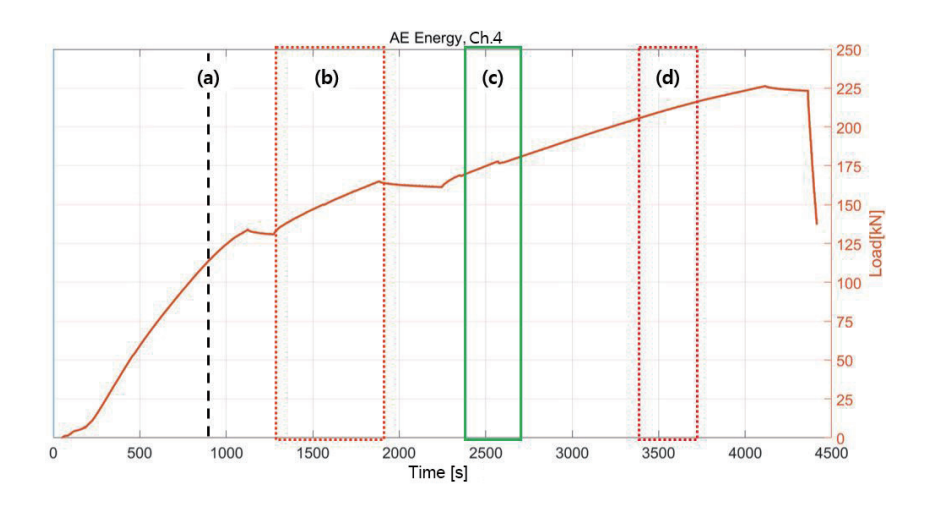


Fig. 13. (Color online) Loading cycle: (a) 110 kN, concrete crack starts to grow; (b) 140–160 kN, concrete crack growth; (c) 170–180 kN, steel wire break; (d) 200–210 kN, predictive void grouting event.

concrete cracks or strand rupture were observed at this location. Given that the signal occurred after the strand rupture, it is presumed to be a secondary signal caused by the broken strand moving and impacting the voids within the grout or sheath.

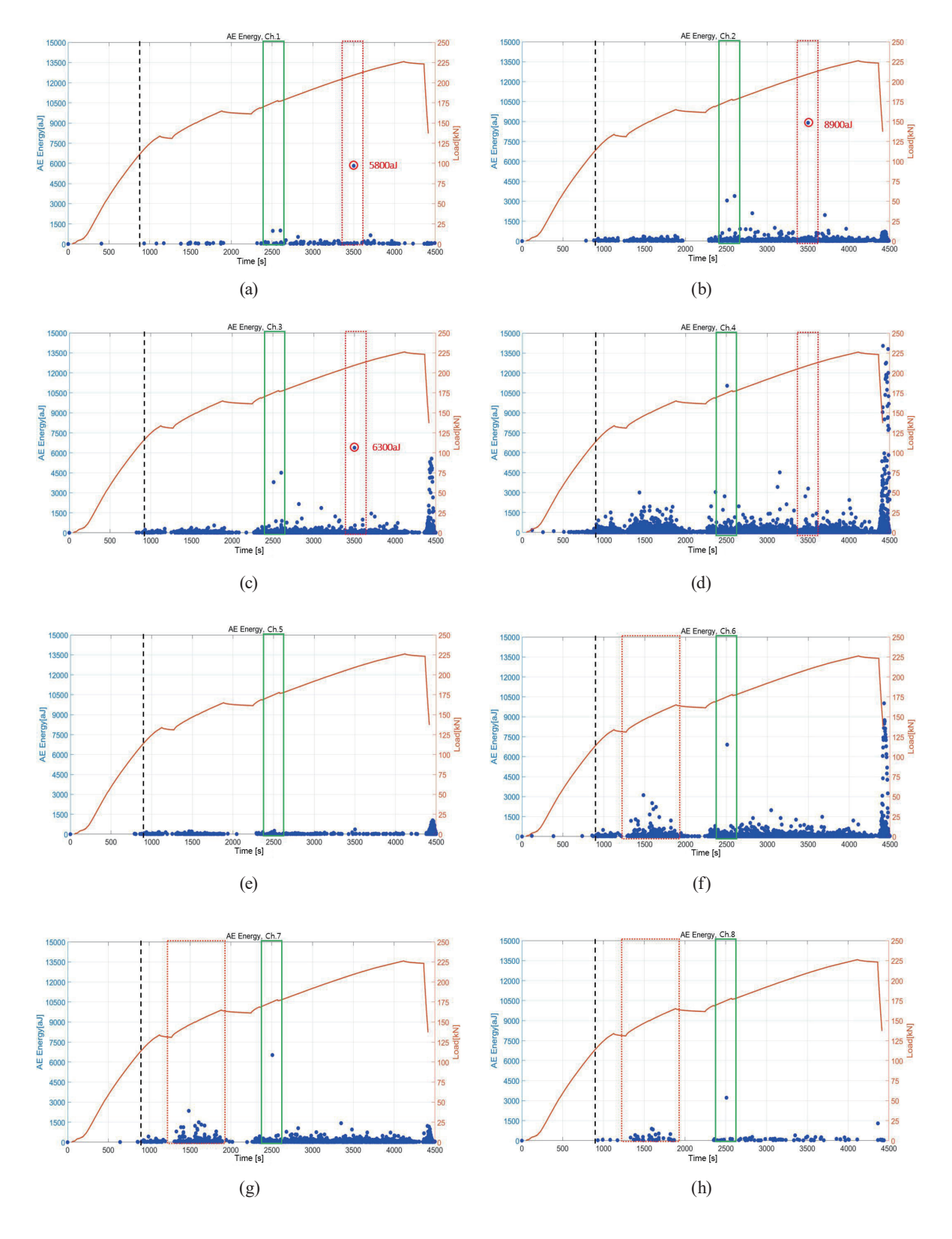


Fig. 14. (Color online) AE energy trends for PSC specimens in void grouting detection test: (a) ch.1, (b) ch.2, (c) ch.3, (d) ch.4, (e) ch.5, (f) ch.6, (g) ch.7, and (h) ch.8 trends.

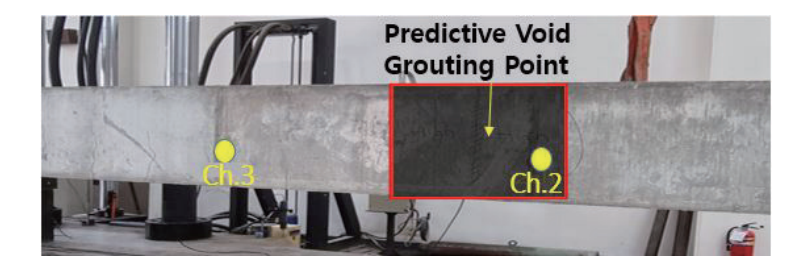


Fig. 15. (Color online) PSC specimen in void grouting detection test (predictive void grouting point).

After the experiment, the PSC specimen was dismantled to inspect the internal tendon condition. The void location identified through measurements was near ch.2, as shown in Fig. 15. Upon inspection, it was confirmed that strands inside the tendon were in direct contact with the sheath pipe, as can be seen in Fig. 16, without being fully covered by grout. As illustrated in Fig. 17, at the bending sections of the tendon, the strands experience downward force due to prestressing, reducing the gap between the sheath pipe and the strands. Consequently, the amount of grout filling this gap naturally decreases. The actual inspection revealed that the sheath pipe and strands were in direct contact, with the missing grout forming voids.

When a load was applied to the structure with direct contact between the sheath pipe and the strands, friction occurred owing to the movement of the strands or the entire tendon. The elastic waves generated by this friction were detected by the AE sensors, creating the high AE energy signals shown in Fig. 13(d). Similarly, the significant increases in AE hits at ch.6 and ch.7, shown in Fig. 13(b), which were unrelated to concrete cracking, are believed to have been caused by the same phenomenon.

2.2.3 Experiment summary

The AE energies recorded at the moment of tendon fracture varied across the different experimental setups, as summarized in Table 6. The highest AE energy, approximately 50000 aJ, was observed in controlled PSC specimens (1), representing direct and relatively unattenuated tendon break signals.

In the case of the PSC I Type girder (2), which involved a decommissioned actual bridge, the AE energies ranged from 10000 to 40000 aJ. Unlike in controlled laboratory specimens, these lower and more variable energy levels primarily reflect the effects of aging and corrosion on the tendon and surrounding materials, which can alter the fracture behavior and attenuate AE signals. This emphasizes the importance of considering material degradation in field applications.

For tendon voids within PSC structures (3), the AE energy was generally lower, around 10000 aJ, with secondary signals caused by voids measuring about 5000 aJ. These secondary signals indicate energy releases related to void-induced microstructural effects, which tend to be weaker and delayed compared with primary tendon breaks.



Fig. 16. (Color online) Specimen inner tendon after load test.

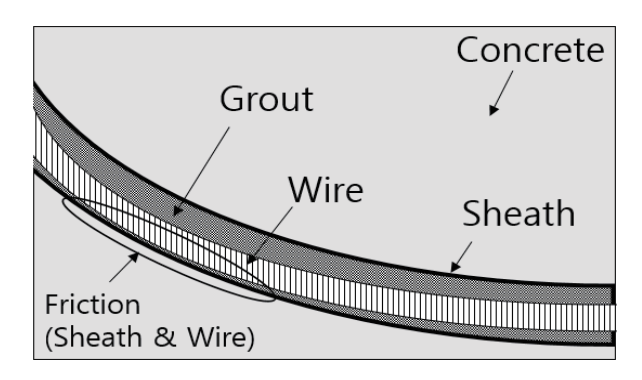


Fig. 17. (Color online) AE event due to sheath and wire friction.

Table 6
AE energy at the break of tendon in each experiment.

| No. | Event | AE Energy (aJ) | Note |
|-----|--------------------------------|----------------|---|
| (1) | PSC specimens | ~50000 | |
| (2) | PSC I Type girder | 10000~40000 | |
| (3) | Tendon voids in PSC structures | ~10000 | Secondary signal due to void ~5000 (aJ) |

Overall, these results suggest that AE energy magnitude not only helps differentiate major tendon fractures from secondary defects but also reflects the effects of aging and corrosion on signal characteristics in real-world bridges. Such findings provide a practical foundation for setting thresholds in monitoring systems that account for the condition of the structure.

2.3 Phase III experiment

2.3.1 Overview of field application

The field application aims to determine the type, quantity, and installation locations of AE sensors and establish an AE-based monitoring system for tendon rupture detection in PSC bridges. To ensure an efficient system for aging PSC bridges, a preliminary site survey was

conducted to prioritize installation locations. The AE system was deployed in selected critical maintenance zones, allowing for systematic monitoring. Ultimately, the AE system provides a web-based monitoring service, enhancing user accessibility, operational convenience, and efficient facility maintenance.

2.3.2 Prioritization of AE system implementation for PSC internal tendons

2.3.2.1 PSC internal tendon damage mechanism

The fundamental mechanisms leading to damage in PSC internal tendons are as follows.

- (1) Surface damage (e.g., pavement cracks, waterproofing layer damage, epoxy joint deterioration)
- (2) Ingress of water (including rainwater and snowmelt containing de-icing agents)
- (3) Grout contamination (or water accumulation in voids)
- (4) Strand corrosion
- (5) Sectional loss or rupture of strands due to corrosion

Figure 18 illustrates the corrosion mechanism of horizontal tendons in a PSC box girder bridge. Cracks in the bridge pavement, defective construction joints, waterproofing layer damage, and epoxy joint deterioration result in water infiltration. The infiltrating water causes duct corrosion or compromises the water tightness of rubber seals at the joints, allowing moisture and chloride ions to enter the tendon. Eventually, this leads to grout contamination and strand corrosion near the joints.

The defects in PSC internal tendons are categorized into four types, excluding strand rupture, which is not a diagnostic target but rather a repair issue.

- (1) Corrosion (including minor section loss)
- (2) Grout voids
- (3) Water leakage
- (4) Crack detection

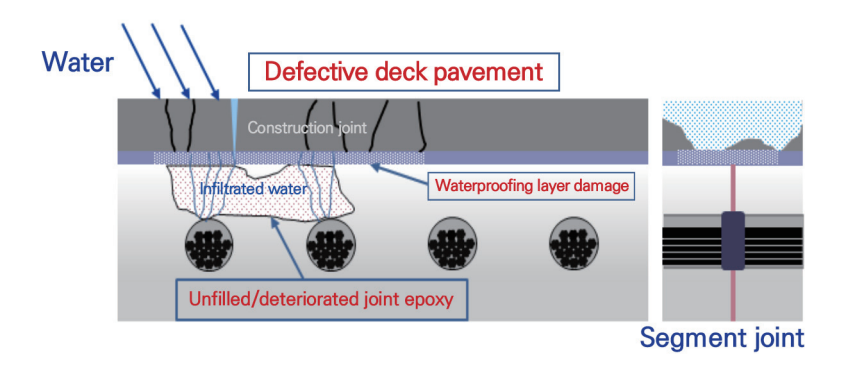


Fig. 18. (Color online) Example of PSC internal tendon damage mechanism.

2.3.2.2 Deriving AE system implementation priorities based on inspection results

The construction priority of the AE system is determined according to the order shown in Fig. 19. The section where corrosion exists or is likely to exist and thus has a high possibility of fracture is set as the highest priority. The next priority is set in the order of causes that can cause corrosion, such as grout, leakage, and cracks.

2.3.2.3 Preliminary survey results

A condition assessment was conducted on the upper horizontal internal tendons of certain sections of elevated roads in Seoul. The pavement and waterproofing layer at each survey location were partially removed, the tendons inspected, and the site restored on the same day.

(1) Survey Location 1: The results of the investigation are as shown in Fig. 20. see page of infiltrating water during drilling with cross-sectional loss due to the corrosion of one strand

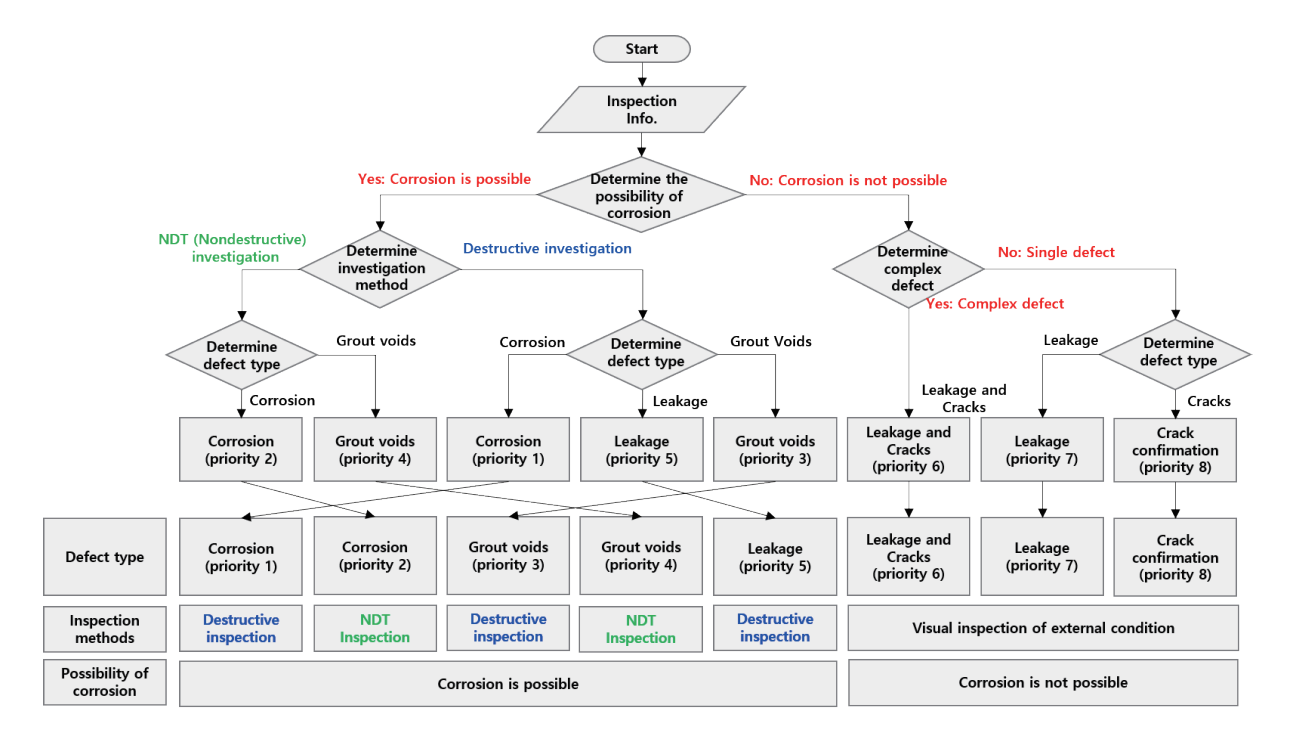


Fig. 19. (Color online) Deriving AE system implementation priorities based on inspection results.

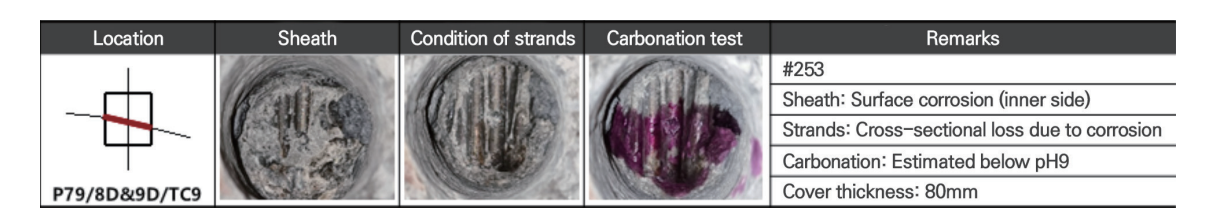


Fig. 20. (Color online) Survey location 1.

of the tendon (in contact with the sheath; surface corrosion on the inner side of the sheath with pH reduction; additional investigation required inside the girder (upward drilling needed)].

(2) Survey Location 2: The results of the investigation are as shown in Fig. 21. [minor cross-sectional loss due to the corrosion of three strands of the tendon (in contact with the sheath at the rubber ring boundary); surface corrosion on the inner side of the sheath, but pH remains stable].

2.3.2.4 Selection of AE monitoring system installation sites

On the basis of the preliminary site survey results, additional inspections were conducted around the areas where corrosion was detected. A visual inspection was performed to identify signs of rust (corrosion traces), efflorescence, water leakage, and cracks, which were used to determine suitable installation locations for the AE sensors.

As observed in the preliminary survey, defects were found mainly at the segment joints. A total of five locations were selected for sensor installation. Additionally, an imported system will be installed at a section close to the gateway (near the power source) for comparative verification. Table 7 presents the number of sensors and the reasons for selecting each installation location (based on visually identified defect traces).

2.3.3 Field application of AE monitoring system

2.3.3.1 System configuration and installation

The AE monitoring system for PSC bridges is configured as shown in Fig. 22. The core components installed on the bridge include AE sensors, AE acquisition terminals, and a gateway.

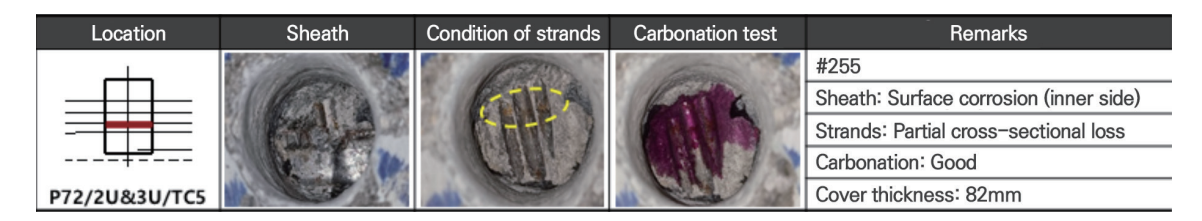


Fig. 21. (Color online) Survey location 2.

Table 7
Sensor installation details by location.

| Installation location | No. of sensors | Reason for selection |
|-----------------------|----------------|--|
| (1) | 4 | Keyseg location, efflorescence and rust observed |
| (2) | 3 | Keyseg location, efflorescence observed |
| | | Corner section, efflorescence observed |
| (3) | 4 | Water accumulation on the floor confirmed |
| | | Identified as a vulnerable location |
| (4) | 3 | Efflorescence and rust observed |
| | | Concrete delamination confirmed |
| (5) | 4 | Keyseg location, efflorescence and rust observed |
| Total | 18 | |

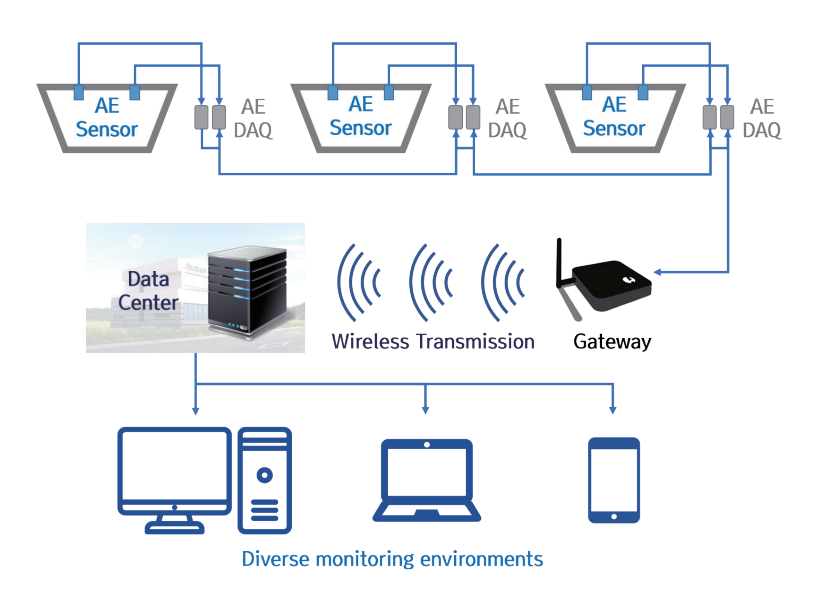


Fig. 22. (Color online) System configuration.

The AE sensors are installed directly on the concrete surface to detect the sound of tendon fractures. The AE data acquisition unit collects signals from the sensors and generates data (AE characteristic parameters). The gateway integrates the data from each AE data acquisition unit and transmits these data wirelessly to the server.

Figures 23–25 show actual on-site installation photos of these three components.

The data transmitted to the server via the gateway are provided to users (actual facility managers) in real time through a web monitoring platform. The web monitoring platform was developed to support access from various environments, including PCs and mobile devices.

2.3.3.2 System application and practical utilization

The web-based monitoring platform provides real-time data visualization, as shown in Fig. 26. It displays the location of the target bridge on a map, with color-coded icons that change according to the signal status level.

Additionally, the recent status history is displayed in the lower-right corner of the screen, as shown in Fig. 27.

Figure 28 shows the detailed screen that appears when a specific bridge location is located. This screen provides the precise installation locations of sensors within the bridge section, the status level of each sensor, and the current measurement data.

The status levels provided to users are determined from experimental results, which are summarized and compiled in Table 8. A threshold of 10000 aJ was set as a reference, and the status levels were classified according to the ratio of measured values to this threshold, as defined in Table 9.



Fig. 23. (Color online) On-site installation of AE sensors.



Fig. 24. (Color online) On-site installation of AE measurement terminal.



Fig. 25. (Color online) On-site installation of gateway.

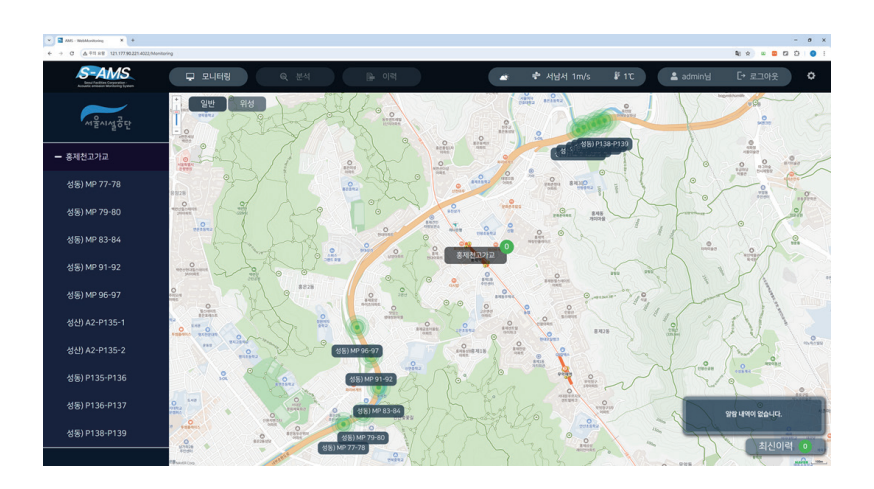


Fig. 26. (Color online) Real-time web monitoring status.



Fig. 27. (Color online) Detailed monitoring screen: recent status history.



Fig. 28. (Color online) Detailed monitoring screen for individual bridge.

Table 8
Basis for threshold setting (summary of experimental results).

| | · . | |
|----------------------|-----|------------------------------|
| Experiment category | | Wire break energy level (aJ) |
| PSC specimen | | Approx. 50000 |
| I girder | | Approx. 10000-40000 |
| Void simulation test | | Approx. 10000 |

Table 9
Detailed definition of condition levels.

| Condition level | Indicator color | Description |
|-----------------|-----------------|--|
| Normal | Green | Within 80% of the threshold |
| Attention | Blue | Between 80 and 100% of the threshold |
| Caution | Yellow | Exceeds threshold but within 110% |
| Danger | Red | Exceeds threshold by more than 110% |
| Disconnected | White | Monitoring unavailable because of communication issues |

2.3.4 Field data status

Since the implementation of the AE monitoring system, no instances of tendon wire strand fractures have been detected. To date, all measured data consist of background noise caused primarily by vehicle-induced vibrations.

2.3.4.1 Annual data trends

Figure 29 is a trend graph that accumulates data for the past year for a specific monitoring section.

An analysis of the annual data (hourly maximum energy trend graph) indicates an increase in noise level caused by vehicle vibrations as temperatures drop. This is likely due to temperature changes on the concrete structures but does not directly correlate with the structural condition of the bridge.

2.3.4.2 Monthly data trends

Figure 30 is a trend graph that accumulates data for one month for a specific monitoring section.

The monthly data (hourly maximum energy trend graph) do not reveal any notable anomalies, with signals remaining relatively consistent throughout the period.

2.3.4.3 Daily data trends

Figure 31 is a trend graph that accumulates data for one day for a specific monitoring section. The daily data (hourly maximum energy trend graph, analyzed alongside traffic volume) show a correlation between signal fluctuations and traffic flow. Overall, the signal fluctuated in accordance with traffic volume and significantly decreased during congestion periods, when vehicle speeds dropped sharply. This suggests that most of the signals detected under normal bridge conditions are caused by vehicle vibrations.

Thus far, the recorded data trends indicate that the majority of signals originate from background noise such as vehicle-induced vibrations. Additional environmental factors such as

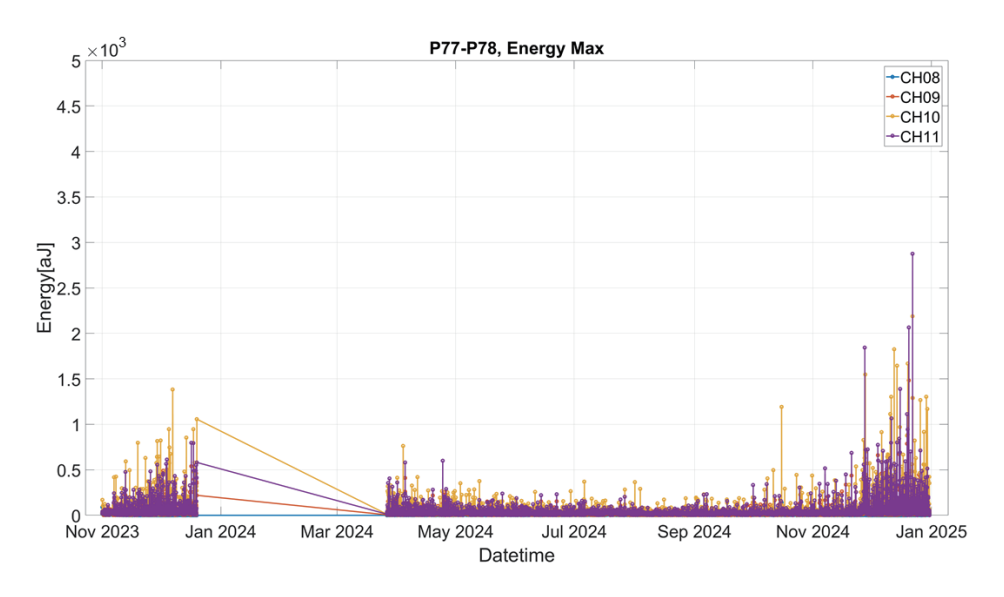


Fig. 29. (Color online) Annual data trends (energy).

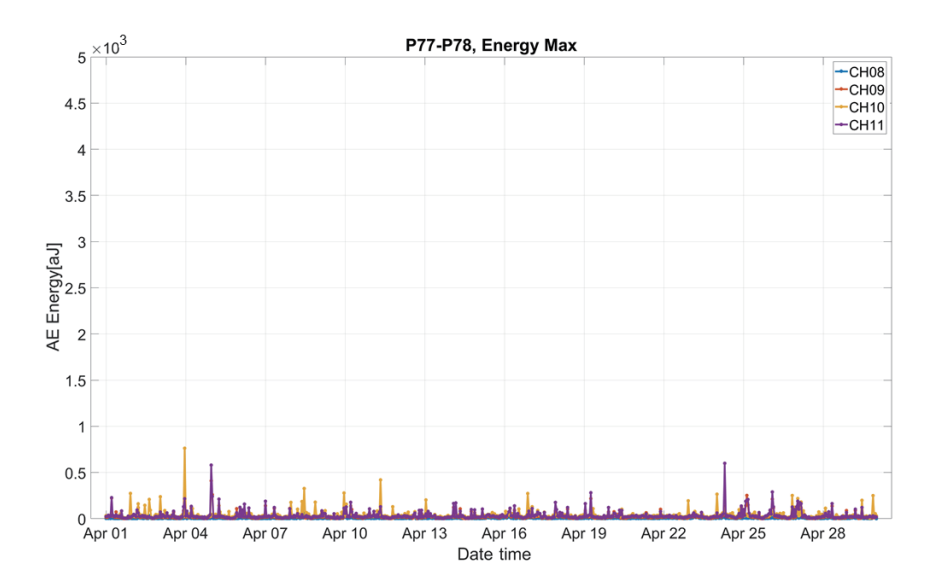


Fig. 30. (Color online) Monthly data trends (energy).

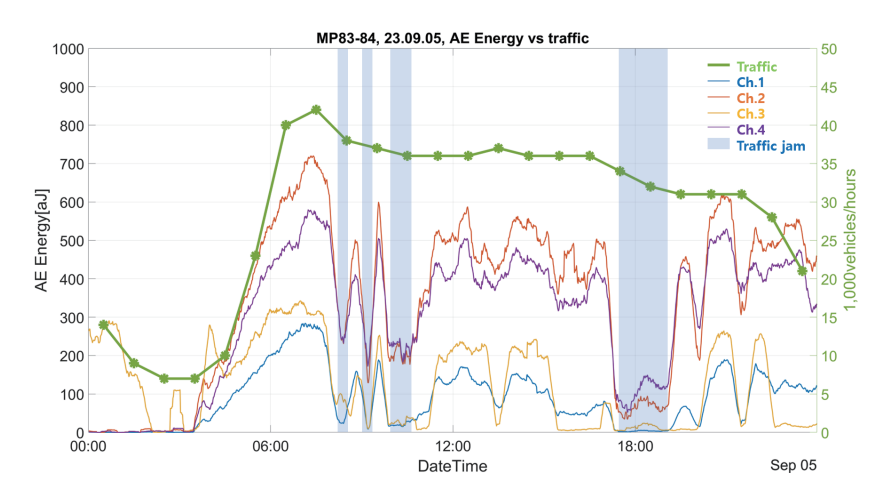


Fig. 31. (Color online) Daily data trends (energy).

wind loads, thermal expansion and contraction, and minor structural movements were also found to contribute to low-energy AE signals. Furthermore, most of the measured signals are below one-tenth of the threshold, making it highly unlikely that they would interfere with the detection of actual tendon wire strand fractures. In addition, these noise signals typically exhibit distinct characteristics—such as low amplitude, short duration, and different frequency content—compared with genuine fracture signals, enabling effective discrimination through signal filtering and pattern recognition algorithms.

3. Conclusion

In this study, a diagnostic technology using AE techniques to detect fractures in the internal tendons of PSC bridges was developed. This study was conducted in three phases: fundamental

experiments, application experiments, and reproducibility tests. From the experimental data, we clearly distinguished internal tendon fracture signals and established maintenance criteria. Finally, AE sensors were installed on an actual bridge, and a real-time monitoring system was implemented and operated for over a year to verify the effectiveness of the proposed technology.

In the fundamental experiments, the characteristics of concrete crack and tendon wire strand fracture signals in PSC structures were analyzed. The results confirmed that AE technology is effective in detecting internal tendon fractures. The application experiments used decommissioned bridges to recreate various potential defect conditions in real-world environments, demonstrating the capability of the system to detect signal attenuation and secondary signals caused by voids. The reproducibility tests ensured consistency in the experimental results and derived reliable criteria for defect signals.

Although the developed AE-based diagnostic technology demonstrates promising capability in detecting internal tendon fractures, there remain potential limitations that warrant careful consideration. Environmental noise, such as traffic-induced vibrations and other background acoustic events, may occasionally generate false signals, leading to possible false positives in monitoring results. Although the current threshold and classification criteria have been designed to minimize these occurrences, the risk of false alarms cannot be completely eliminated.

Moreover, the variability in AE signal characteristics caused by different structural conditions, aging effects, and material heterogeneity introduces challenges in consistently distinguishing fracture signals from benign anomalies. Therefore, future research should focus on refining signal processing algorithms and incorporating advanced AI-based pattern recognition techniques to enhance the accuracy and robustness of fracture detection.

Additionally, long-term monitoring data accumulation will be essential to statistically evaluate false detection rates and to optimize diagnostic criteria for diverse infrastructure environments. Addressing these limitations will further enhance the reliability and practical applicability of AE-based maintenance systems in real-world settings.

The field application results confirmed that the AE monitoring system functions as a practical tool for the real-time detection of internal tendon fractures in PSC bridges. The data-driven classification and warning system significantly improved maintenance efficiency. In particular, the method of distinguishing status levels based on signals exceeding the threshold value (10000 aJ) provided clear guidelines for bridge maintenance.

This study emphasizes the importance of AE sensor technology in detecting tendon fractures embedded in concrete structures. By differentiating AE signals generated by concrete cracking and those from tendon breakage, the research underscores the necessity of signal analysis methods tailored to the material properties of PSC components. These insights directly inform the development of practical, sensor-based monitoring and maintenance systems for long-term infrastructure health assessment.

This study successfully applied AE techniques for internal tendon fracture monitoring in PSC bridges, contributing to the broader adoption of AE technologies in structural maintenance. Furthermore, the diagnostic methodology demonstrated in this study holds significant potential for extension to other types of infrastructure, including cable-stayed bridges, suspension bridges, and offshore structures where internal or inaccessible components are critical to structural integrity.

However, given that the findings are based on specific bridge structures and experimental conditions, further research is needed to extend the application to various structural types and environmental conditions. Future efforts should also focus on refining signal interpretation by integrating domain-specific AE signal databases, improving noise filtering algorithms, and optimizing sensor deployment strategies for different structural configurations.

Future research studies should aim to enhance the accuracy of AE signal interpretation by incorporating AI-based analysis techniques and further improve the reliability and applicability of the diagnostic technology through the accumulation of long-term monitoring data. Ultimately, such improvements will support the development of a versatile AE-based monitoring system adaptable across infrastructure types and maintenance requirements. Building upon this foundation, the next step is to develop an integrated multisensor monitoring system that combines AE with other sensing technologies—such as concrete temperature and vibration sensors—to enable a more comprehensive assessment of structural health.

Acknowledgments

We thank Professor Soo-Jin Cho for his invaluable guidance and support in analyzing the measurement results in this study.

References

- 1 X. Luo, H. Haya, T. Inaba, and T. Shiotani: Soil Dyn. Earthquake Eng. **26** (2006) 1101. https://doi.org/10.1016/j.soildyn.2006.03.002
- 2 A. Behnia, H. K. Chai, and T. Shiotani: Constr. Build. Mater. **65** (2014) 282. https://doi.org/10.1016/j.conbuildmat.2014.04.103
- 3 H. A. Elfergani, R. Pullin, and K. M. Holford: Constr. Build. Mater. 40 (2013) 925. https://doi.org/10.1016/j.conbuildmat.2012.11.071
- 4 C. U. Grosse and M. Ohtsu: Acoustic Emission Testing (Springer, Dordrecht, 2008) pp. 211–238.
- 5 X. Luo, H. Haya, T. Inaba, T. Shiotani, and Y. Nakanishi: Constr. Build. Mater. 18 (2004) 215. https://doi.org/10.1016/j.conbuildmat.2003.10.011
- 6 T. Shiotani: J. Acoust. Emiss. 19 (2001) 118.
- 7 M. Ohtsu: Proc. 24th Int. Acoustic Emission Symposium, T. Shiotani, Y. Mizutani, and H. Yuki, Eds. (The Japanese Society for Non-Destructive Inspection, 2018) pp. 11–16.
- 8 G. Ma and Q. Du: Constr. Build. Mater. **250** (2020) 118860. https://doi.org/10.1016/j.conbuildmat.2020.118860
- 9 R. Janeliukstis, A. Clark, M. Papaelias, and S. Kaewunruen: Eng. Struct. 178 (2019) 493. https://doi.org/10.1016/j.engstruct.2018.10.058
- 10 F. Zhang, G. I. Z. Garnica, Y. Yang, and E. Lantsoght: Sensors 20 (2020) 5622. <u>https://doi.org/10.3390/s20195622</u>
- 11 M. A. Abdelrahman, M. K. ElBatanouny, J. R. Rose, and P. H Ziehl: Res. Nondestr. Eval. 30 (2019) 127. https://doi.org/10.1080/09349847.2018.1426800
- 12 F. A. Barrios and P. H. Ziehl: ACI Struct. J. 112 (2015) 3. http://doi.org/10.14359/51687294
- 13 T. Shiotani, Y. Oshima, M. Goto, and S. Momoki: Constr. Build. Mater. 48 (2013) 1286. https://doi.org/10.1016/j.conbuildmat.2013.04.026
- 14 A. Nair and C. S. Cai: Eng. Struct. **32** (2010) 1704. https://doi.org/10.1016/j.engstruct.2010.02.020
- D. Tonelli, M. Luchetta, F. Rossi, P. Migliorino, and D. Zonta: Sensors 20 (2020) 7272. https://doi.org/10.3390/s20247272
- 16 A. Lange, M. Käding, R. Hinrichs, J. Ostermann, and S. Marx: Proc. EWSHM 2022, P. Rizzo and A. Milazzo, Eds. (Springer, Cham, 2023) pp. 1024–1033. https://doi.org/10.1007/978-3-031-07322-9 104
- 17 M. Käding, G. Schacht, and S. Marx: Eng. Struct. 270 (2022) 114846. https://doi.org/10.1016/j.engstruct.2022.114846
- 18 M. Käding and S. Marx: Appl. Sci. 14 (2024) 3045. https://doi.org/10.3390/app14073045
- 19 S. Farhadi, M. Corrado, O. Borla, and G. Ventura: Comput.-Aided Civ. Infrastruct. Eng. 39 (2024) 186. https://doi.org/10.1111/mice.13079